Mitochondrial anchorage and fusion contribute to mitochondrial inheritance and quality control in the budding yeast *Saccharomyces cerevisiae*

Ryo Higuchi-Sanabria[a], Joseph K. Charalel[a], Matheus P. Viana[b], Enrique J. Garcia[a], Cierra N. Sing[a], Andrea Koenigsberg[a], Theresa C. Swayne[c], Jason D. Vevea[a,†], Istvan R. Boldogh[a], Susanne M. Rafelski[b], and Liza A. Pon[a,c,*]

[a]Department of Pathology and Cell Biology and [c]Herbert Irving Comprehensive Cancer Center, Columbia University, New York, NY 10032; [b]Department of Developmental and Cell Biology and Center for Complex Biological Systems, University of California, Irvine, Irvine, CA 92697

ABSTRACT **Higher-functioning mitochondria that are more reduced and have less ROS are anchored in the yeast bud tip by the Dsl1-family protein Mmr1p. Here we report a role for mitochondrial fusion in bud-tip anchorage of mitochondria. Fluorescence loss in photobleaching (FLIP) and network analysis experiments revealed that mitochondria in large buds are a continuous reticulum that is physically distinct from mitochondria in mother cells. FLIP studies also showed that mitochondria that enter the bud can fuse with mitochondria that are anchored in the bud tip. In addition, loss of fusion and mitochondrial DNA (mtDNA) by deletion of mitochondrial outer or inner membrane fusion proteins (Fzo1p or Mgm1p) leads to decreased accumulation of mitochondria at the bud tip and inheritance of fitter mitochondria by buds compared with cells with no mtDNA. Conversely, increasing the accumulation and anchorage of mitochondria in the bud tip by overexpression of *MMR1* results in inheritance of less-fit mitochondria by buds and decreased replicative lifespan and healthspan. Thus quantity and quality of mitochondrial inheritance are ensured by two opposing processes: bud-tip anchorage by mitochondrial fusion and Mmr1p, which favors bulk inheritance; and quality control mechanisms that promote segregation of fitter mitochondria to the bud.**

Monitoring Editor
Gia Voeltz
University of Colorado, Boulder

Received: Jul 1, 2015
Revised: Jan 6, 2016
Accepted: Jan 7, 2016

INTRODUCTION

Studies dating from the 1950s indicate that mitochondria are selectively localized to sites of high ATP utilization and/or calcium homeostasis. The earliest studies revealed that mitochondria are enriched in the neuronal synapse (Palay, 1956). Mitochondria also accumulate in the bud tip of the budding yeast *Saccharomyces cerevisiae* and in the immunological synapse that forms between T-cells and antigen-presenting cells during T-cell activation (Yang *et al.*, 1999; Quintana *et al.*, 2007). Other studies revealed that localization of mitochondria to their site of action affects cellular function. Specifically, defects in localization of mitochondria to the neuronal synapse, immunological synapse, and yeast bud tip result in defects in neuronal transmission and plasticity, T-cell activation, and yeast daughter cell fitness and lifespan, respectively (Stowers *et al.*, 2002; Guo *et al.*, 2005; Verstreken *et al.*, 2005; Quintana *et al.*, 2007; McFaline-Figueroa *et al.*, 2011). Here we investigated the role of mitochondrial fusion in anchorage of mitochondria in the yeast bud tip and mitochondrial quality control during yeast cell division.

The mechanisms underlying site-specific anchorage of mitochondria at neuronal and immunological synapses are not well understood. However, recent studies indicate that mitochondria in the yeast bud tip are anchored to cortical endoplasmic reticulum (cER), which is anchored to the plasma membrane (Swayne *et al.*, 2011). These studies also revealed a role for Mmr1p, a member of the DSL family of tethering proteins, for anchorage of mitochondria to cER in

This article was published online ahead of print in MBoC in Press (http://www.molbiolcell.org/cgi/doi/10.1091/mbc.E15-07-0455) on January 13, 2016.

†Present address: Department of Neuroscience, University of Wisconsin, Madison, WI 53705.

*Address correspondence to: Liza A. Pon (lap5@cumc.columbia.edu).

Abbreviations used: FLIP, fluorescence loss in photobleaching; mtDNA, mitochondrial DNA; *rho*^{0} cells, yeast with no mtDNA; *rho*$^+$ cells, yeast with wild-type mtDNA; RACF, retrograde actin cable flow.

the yeast bud tip. Mmr1p was originally identified as a protein that can bind to mitochondria and to Myo2p, a type V myosin that mediates transport of cargoes from mother cells to bud cells (Itoh *et al.*, 2004). *MMR1* also has genetic interactions with *MYO2* (Eves *et al.*, 2012; Chernyakov *et al.*, 2013). Because deletion of *MMR1* has no effect on mitochondrial movement in mother cells (Swayne *et al.*, 2011) and *MMR1* protein and mRNA are enriched in the bud tip (Shepard *et al.*, 2003), it is possible that Mmr1p is a cargo adapter that links Myo2p to mitochondria for movement across the bud neck and within the bud. Other studies support an additional function for Mmr1p in the bud. Mmr1p localizes to a limited number of punctate structures at sites of interaction of mitochondria and cER in the yeast bud tip, is recovered with mitochondria and ER by subcellular fractionation, and is required for anchorage of mitochondria in the bud tip (Swayne *et al.*, 2011). These findings indicate that Mmr1p plays a direct role in linking mitochondria to cER in the yeast bud tip in addition to its function in movement of mitochondria in buds.

Mmr1p is also required for mother–daughter age asymmetry, the conserved process by which offspring are born young, largely independent of the age of their parents. In budding yeast, this age asymmetry is achieved by segregation of aging determinants between mother and daughter cells, which allows for continued aging of mother cells and rejuvenation of daughter cells (Mortimer and Johnston, 1959; Egilmez and Jazwinski, 1989; Kennedy *et al.*, 1994; Sinclair and Guarente, 1997). Previous studies indicated that mitochondria are aging determinants that are asymmetrically inherited during yeast cell division. Mitochondria that are anchored in the yeast bud tip and destined for inheritance by yeast daughter cells have less superoxide and a more-reducing redox potential than mitochondria in the mother cell. Moreover, defects in inheritance of fitter mitochondria by yeast daughter cells affect daughter-cell lifespan and mother–daughter age asymmetry (McFaline-Figueroa *et al.*, 2011; Higuchi *et al.*, 2013). Of interest, mitochondria are also asymmetrically inherited in mammalian cells: old and young mitochondria are segregated during division of human mammary stem–like cells, and cells that inherit fewer old mitochondria retain their stem-like traits (Katajisto *et al.*, 2015). Thus there is evidence that mitochondria are asymmetrically inherited during cell division and that this affects cell fitness and fate in yeast and other eukaryotes.

The mechanism underlying asymmetric inheritance of mitochondria in mammary stem–like cells is not well understood. However, recent evidence indicates that preferential inheritance of higher-functioning, more-acidic vacuoles by yeast daughter cells creates an environment that augments mitochondrial membrane potential at that site (Hughes and Gottschling, 2012; Henderson *et al.*, 2014). Other studies indicate that organelle–cytoskeleton interactions that drive mitochondrial movement contribute to segregation of mitochondria according to fitness in dividing yeast cells and inheritance of higher-functioning mitochondria by yeast daughter cells. Actin cables of budding yeast are bundles of F-actin that serve as tracks for bidirectional cargo transport. Actin cables also undergo continuous movement from buds toward mother cells (Yang and Pon, 2002), which pushes actin cable–associated cargoes including mitochondria away from the bud. As a result, retrograde actin cable flow (RACF) serves as a filter to prevent lower-functioning, less-motile mitochondria from entering the bud and as a force generator to clear lower-functioning mitochondria from the bud. Indeed, increasing the rate of RACF results in increased fitness of mitochondria inherited by buds, and this increase in mitochondrial fitness leads to extended replicative lifespan and increased cellular healthspan (Higuchi *et al.*, 2013).

Here we identify a novel role for mitochondrial fusion in regulation of mitochondrial quantity and quality control during inheritance. Fzo1p and Mgm1p are conserved GTPases that localize to and are required for fusion of mitochondrial outer and inner membranes, respectively, interact with each other, and mediate tethering of mitochondrial membranes to one another during mitochondrial fusion (Hermann *et al.*, 1998; Meeusen *et al.*, 2006). Both proteins are required for maintaining the tubular mitochondrial reticulum and affect mitochondrial function, in part because they are required for maintenance of mitochondrial DNA (mtDNA; Hermann *et al.*, 1998; Rapaport *et al.*, 1998; Koshiba *et al.*, 2004). We find that mitochondria entering the bud fuse with mitochondria that are anchored in the bud tip, and this fusion contributes to anchorage and accumulation of mitochondria in the bud tip. Moreover, promoting anchorage of mitochondria in the yeast bud tip compromises mitochondrial quality control during yeast cell division and promotes inheritance of less-fit mitochondria by yeast daughter cells.

RESULTS

Mitochondria in large buds are a continuous reticulum that is physically distinct from mitochondria in mother cells

Mitochondria in budding yeast have been described as a single continuous reticulum. However, recent studies revealed that mitochondria in the mother cell of budding yeast are physically and functionally distinct from each other and from mitochondria in the bud (McFaline-Figueroa *et al.*, 2011). Here we used fluorescence loss in photobleaching (FLIP) to assess mitochondrial continuity in wild-type yeast at late stages in the cell division cycle. In these FLIP studies, a small area is photobleached repeatedly in mitochondria that contain mitochondrial matrix–targeted green fluorescent protein (Cit1-GFP). As diffusion brings fresh fluorophores into the targeted area and photobleached fluorophores out of the targeted area, fluorescence is lost from all fluorophores that are in the matrix of a single continuous mitochondrion.

We find that repeatedly photobleaching a region on a mitochondrion in the tip of a large bud results in rapid loss of fluorescence of Cit1-GFP in the targeted area and in a region of mitochondria adjacent to the photobleached zone (Figure 1, A and B). Subsequently, fluorescence is also lost from mitochondria throughout the bud. Indeed, 97% of GFP fluorescence is lost in mitochondria in large buds during the 48-s period analyzed. However, fluorescence persists in mitochondria in the mother cell.

To further characterize mitochondrial continuity, we carried out quantitative analysis of the three-dimensional (3D) skeletons of mitochondrial networks (Rafelski *et al.*, 2012) from spinning-disk confocal *z*-stacks of live yeast cells expressing mitochondrial matrix–targeted GFP. We found that the length of the longest continuously connected mitochondrion remains unchanged in the mother cell as a function of bud size. In contrast, the length of the longest continuously connected mitochondrion in buds increased as a function of bud size (Figure 1C). Moreover, the percentage of cells where mitochondria in the bud are connected to mitochondria in the mother cell decreased with increasing bud size (Figure 1D). Thus, as bud cells increase in size, mitochondria in the bud become more physically distinct from mitochondria in mother cells. Of interest, 80% of the total mitochondrial volume in large buds is part of a single, continuous reticulum (Figure 1E). In contrast, only 60% of the total mitochondrial volume forms the largest connected component in mother cells.

These data, together with our FLIP experiments, provide additional evidence that mitochondria in the mother and bud compartments are physically distinct from each other in yeast bearing large

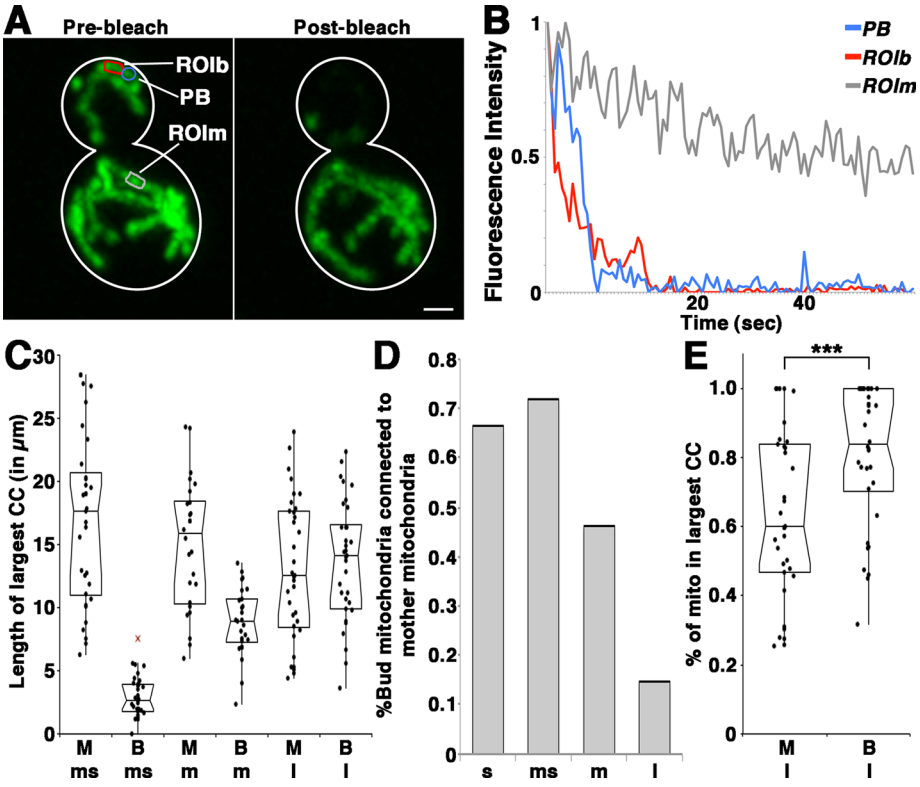

FIGURE 1: Mitochondria in large buds are a single continuous reticulum that is physically distinct from mitochondria in the mother. (A) Wild-type yeast expressing mitochondrial matrix–targeted GFP. A 0.35-μm^2 spot on a mitochondrion in the bud tip of a yeast cell bearing a large bud (60–80% of mother cell size) was subjected to continuous illumination at 488 nm. Photobleaching and confocal imaging of GFP-labeled mitochondria were carried out continuously for 48 s. Images are maximum projections of cells before and after photobleaching. *Z*-series were captured throughout the entire cell at 0.3-μm intervals. PB, photobleached area (blue); ROIb (red) and ROIm (gray), regions of interest in the bud and mother cell, respectively, in which GFP intensity was measured. Scale bar, 1 μm. (B) Integrated intensity of mitochondrial matrix–targeted GFP as a function of time of photobleaching in the photobleached zone (blue) and in ROIs in the bud (ROIb; red) and mother cell (ROIm; gray). Values are normalized to the value of each ROI at time 0. (C) The length of the largest connected component (CC) in the bud increases as the bud grows. Notched dot-box plot of the length of the largest connected components in cells with different-sized buds. The central band in the box represents the median, and boxes indicate the middle quartiles; whiskers extend to the 5th and 95th percentiles, and red crosses indicate outliers (defined as quartile 1 – 1.5× interquartile range and quartile 3 + 1.5× interquartile range). Bud sizes are as follows: ms (medium-small; $n = 33$), m (medium; $n = 26$), and l (large; $n = 34$) as defined in *Materials and Methods*. (D) The percentage of buds in each bud-size category with mitochondria that are connected to mitochondria in the mother. $n = 18$, 32, 26, and 34 for small (s), medium-small (ms), medium (m), and large (l) buds, respectively. Cells with no mitochondria in the bud were excluded. (E) Notched dot-box plot of the connectivity of the mitochondrial network, measured as the length of the largest connected component divided by the total length of mitochondria in the cell. ***$p = 0.0019$ using nonparametric Wilcoxon signed-rank testing. $n = 34$.

buds (McFaline-Figueroa *et al.*, 2011). Equally important, our data indicate that the mitochondrial network in large buds is more interconnected to itself than is the network in mother cells. Thus we obtained evidence that mitochondria in large buds, that is, in daughter cells at late stages in cell division before cytokinesis, are primarily a single continuous reticulum.

We next performed FLIP experiments in yeast with mutations in mitochondrial fusion and fission genes (*DNM1* and *FZO1*; Figure 2). In *fzo1*Δ cells, continuous photobleaching of a 0.25-μm^2 region on a mitochondrion in large buds resulted in loss of fluorescence of Cit1-GFP in the photobleached organelle within 15 s but not in other mitochondria in the bud or mother cell during the 25-s period analyzed. Our FLIP experiments can resolve the fragmented mitochondria of *fzo1*Δ cells and provide evidence that mitochondria within the buds of *fzo1*Δ cells are not a continuous reticulum, in contrast to wild-type cells.

In contrast, continuous photobleaching of a region on a mitochondrion in large buds of *dnm1*Δ or *dnm1*Δ *fzo1*Δ cells resulted in a loss of Cit1-GFP fluorescence in mitochondria in the bud and mother cells. In the *dnm1*Δ mutant, there is an equal loss of fluorescence of Cit1-GFP in mother cells and buds. Thus mitochondria in these cells are a single continuous reticulum during the time frame of our FLIP analysis. There is also a loss of fluorescence in mother cells in *dnm1*Δ *fzo1*Δ cells; however, the loss of fluorescence in buds is greater than that observed in mother cells. Thus mitochondria in bud and mother cells are more interconnected in *dnm1*Δ *fzo1*Δ cells than with wild-type cells but not to the same extent as mitochondria in *dnm1*Δ cells.

A role for mitochondrial fusion in accumulation of mitochondria in the bud tip

To test whether mitochondria that enter the bud can fuse with mitochondria that are anchored in the bud tip, we carried out simultaneous photobleaching in mitochondria in the bud tips of two cells (Figure 3A). In one cell, the mitochondrion in the tip of a large bud was a continuous reticulum and physically separated from mitochondria in the mother cell: continuous photobleaching of a zone on mitochondria in the bud tip resulted in loss of Cit1-GFP fluorescence in all mitochondria in the bud tip and no loss of fluorescence in mitochondria in the mother cell. In the other cell, the mitochondrial reticulum in the tip of a large bud was physically separate from the mitochondria in the mother cell at the start of photobleaching but was connected to one mitochondrion in the mother cell at the end of the imaging period (Figure 3A, arrowhead). Here there was a loss of fluorescence within all the mitochondria in the bud tip and in one tubular mitochondrion in the mother cell that was not physically associated with mitochondria in the bud at the start of the FLIP analysis.

Our interpretation of these findings is that the tubular mitochondrion moved from the mother cell to the bud and fused with mitochondria that accumulated in the bud tip. Because GFP was targeted to the mitochondrial matrix, the observed fusion occurs across mitochondrial outer and inner membranes. Finally, because mitochondrial fusion–linked loss of fluorescence with photobleaching occurred in some but not all mitochondria in the mother cell, it is clear that mitochondria in the mother cell are not a continuous reticulum on the time scale of these experiments (~1 min). Thus mitochondria that enter the bud can fuse with mitochondria that

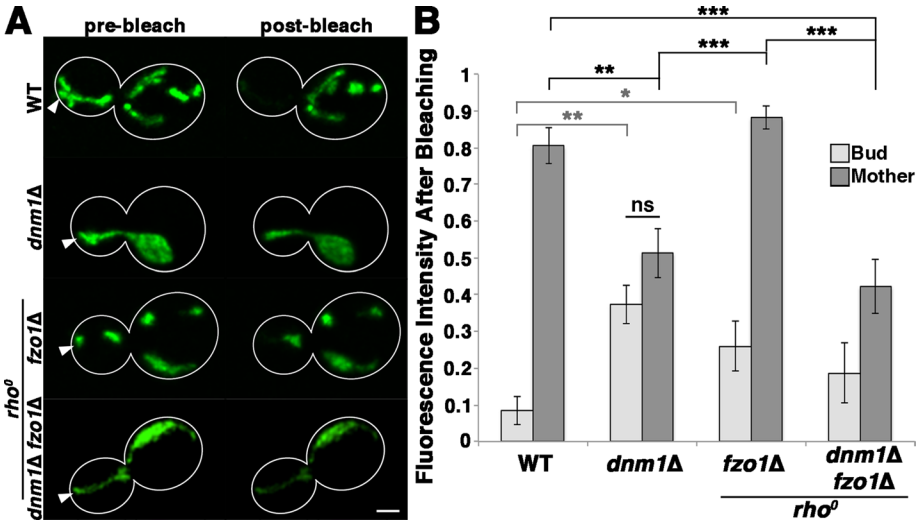

FIGURE 2: Mitochondrial continuity in large buds of *fzo1*Δ *dnm1*Δ and *dnm1*Δ *fzo1*Δ cells. (A) Cit1-GFP in wild-type, *dnm1*Δ, *fzo1*Δ *rho*^{0}, and *dnm1*Δ *fzo1*Δ *rho*^{0} yeast cells after continuous photobleaching of a region of interest in mitochondria in the bud. Arrow points to the photobleaching site. A 0.25-μm^2 spot on a mitochondrion in the bud tip of a yeast cell bearing a large bud (60–80% of mother cell size) was subjected to continuous illumination at 405 nm. Photobleaching and confocal imaging of GFP-labeled mitochondria were carried out continuously for 25 s. (B) Loss of fluorescence of mitochondria in bud and mother cells after continuous photobleaching of a portion of mitochondria in the bud. Integrated intensity after photobleaching in bud and mother cells was normalized to prebleaching integrated intensity. ns = *p < 0.05, **p < 0.01, and ***p < 0.001 using Student's t test. The p values comparing fluorescence intensity remaining after photobleaching in bud vs. mother cells were calculated using Student's t test: wild type, >0.001; *dnm1*Δ, 0.092; *fzo1*Δ, >0.001; and *dnm1*Δ *fzo1*Δ, 0.047. Data are pooled from three independent trials; 9–18 cells/strain. Scale bar, 1 μm.

accumulate and are anchored in the bud tip, which, in turn, results in formation of a continuous mitochondrial reticulum in the bud tip.

Next we tested whether mitochondrial fusion contributes to anchorage and accumulation of the organelle in the bud tip. To do so, we studied the effect of deletion of *FZO1* on the relative mitochondrial volume as a function of location within yeast cells. Because deletion of *FZO1* also results in loss of mitochondrial DNA (mtDNA), we also studied mitochondrial inheritance in yeast with no mtDNA (*rho*^{0} cells). Here the *rho*^{0} cell was produced by deletion of *MGM101*, which results in rapid loss of mtDNA due to defects in mtDNA recombination repair (Supplemental Figure S1; Chen *et al.*, 1993). We observe a 60% decrease in accumulation of mitochondria in the bud tip in *fzo1*Δ cells compared with wild-type cells (Figure 3, B and C, and Supplemental Figure S2). The observed defect in mitochondrial accumulation at the bud tip in *fzo1*Δ cells is not due to their function in maintenance of mtDNA: in *mgm101*Δ cells, which are also *rho*^{0}, mitochondria accumulate in the bud tip to the same extent as in wild-type cells (Figure 3C).

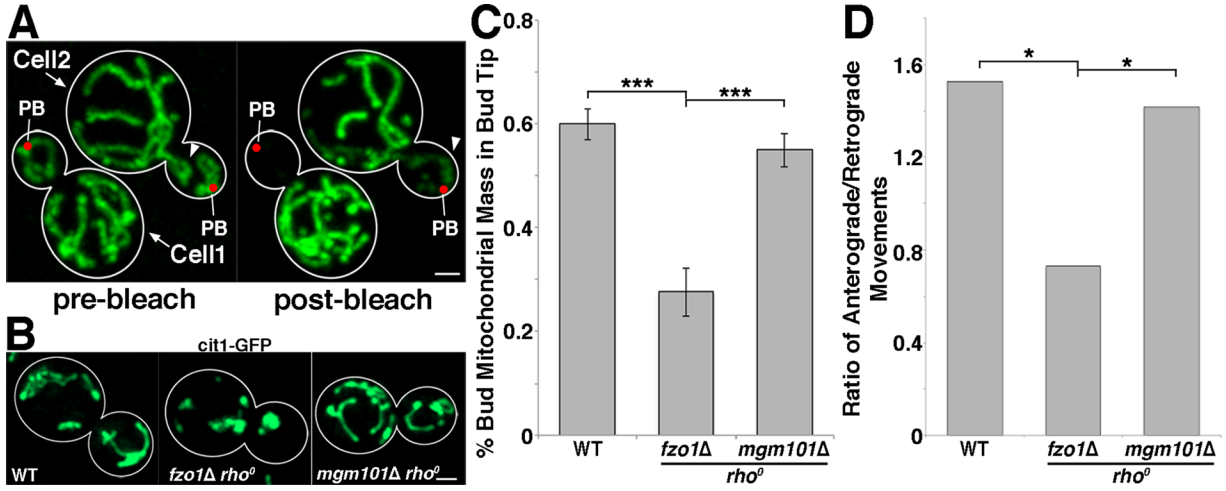

FIGURE 3: Mitochondrial fusion is required for accumulation of mitochondria at the bud tip. (A) Simultaneous photobleaching and imaging of a 0.44-μm^2 region of mitochondria in the bud tip in two wild-type cells (cells 1 and 2) was carried out as for Figure 1. Red spot, photobleached zone. White arrowhead indicates a mitochondrion that fuses with mitochondria in the bud tip in cell 2. Scale bar, 1 μm. (B–D) Mitochondrial accumulation in the bud tip was assessed. (B) Representative images of wild-type, *fzo1*Δ *rho*^{0}, and *mgm101*Δ *rho*^{0} cells, as indicated, expressing Cit1-GFP in glucose-based medium. (C, D) Quantification of mitochondrial accumulation in the bud tip. Integrated intensity of Cit1-GFP fluorescence was measured in the half of the daughter cell distal to the neck relative to integrated intensity of the entire daughter cell in large-budded wild-type, *fzo1*Δ *rho*^{0}, and *mgm101*Δ *rho*^{0} cells in glucose-based medium. (D) Further analysis of mitochondrial motility was performed in the bud tip. The bud tip is defined as the half of the bud distal to the neck. Images were captured every 1 s for 30 s in a single focal plane slightly above the center of the mother cell. Frequency of anterograde and retrograde mitochondrial movements in the bud tip was quantified in wild-type, *fzo1*Δ *rho*^{0}, and *mgm101*Δ *rho*^{0} cells in medium- to large-budded cells (bud-to-mother diameter ratio of 0.4–0.8) in glucose-based medium. Values shown are ratios of anterograde to retrograde movements. Data are pooled from three independent trials; 71–109 cells/strain. *p < 0.05 and ***p < 0.001 based on chi-square testing.

To distinguish the role of fusion from other effects of deletion of *FZO1* on the mitochondrial network, we studied bud-tip accumulation of mitochondria in *mgm1*Δ cells, which have defects in mitochondrial inner membrane fusion and maintenance of mtDNA, and in *dnm1*Δ *fzo1*Δ cells. Mitochondria in *dnm1*Δ *fzo1*Δ cells exhibit defects in fusion but do not exhibit the severe morphology defects observed in *fzo1*Δ or *mgm1*Δ cells (Supplemental Figure S3). Moreover, unlike *fzo1*Δ or *mgm1*Δ cells, which are always *rho*^{0}, *dnm1*Δ *fzo1*Δ cells maintain mtDNA if they are propagated using media based on a nonfermentable, glycerol-based carbon source (Supplemental Figure S1; Bleazard *et al.*, 1999). We observe a defect in accumulation of mitochondria in the bud tip in *mgm1*Δ (Supplemental Figure S4, A–C) and *dnm1*Δ *fzo1*Δ (Supplemental Figure S3) cells, similar to that observed in *fzo1*Δ cells, and this defect is independent of the presence or absence of mtDNA in those cells.

To determine whether defects in accumulation of mitochondria in the bud tip in mitochondrial fusion mutants are due to impaired anchorage of the organelle at that site, we studied the frequency of anterograde and retrograde mitochondrial movement at the bud tip. In wild-type cells, mitochondria undergo anterograde movement into the bud tip, and mitochondria that are not anchored at that site undergo RACF-driven retrograde movement, which pushes them away from the bud tip. Thus the ratio of anterograde to retrograde mitochondrial movements in the bud tip is an indicator of anchorage of the organelle at that site. In wild-type cells, 60% of mitochondrial movements in the tip of the large bud are anterograde and 40% are retrograde (Figure 3D). In contrast, in *fzo1*Δ and *dnm1*Δ *fzo1*Δ mutants, 100% of the mitochondria observed to enter the tip of a large bud fail to anchor there and instead undergo retrograde movement away from the bud (Figure 3D; Supplemental Figure S5). Thus loss of mitochondrial fusion results in a defect in anchorage of mitochondria in the bud tip and a resultant increase in net retrograde movement of mitochondria within the bud. This defect in bud- tip anchorage is not observed in *dnm1*Δ or *rho*^{0} (*mgm101*Δ) cells (Figure 3D and Supplemental Figure S5). Thus the bud-tip accumulation defect observed in *fzo1*Δ and *dnm1*Δ *fzo1*Δ cells is due to defects in anchorage of mitochondria at that site.

Inhibition of fusion affects mitochondrial function

Mitochondrial function was assessed using 3,3′-dihexyloxacarbocyanine iodide ($DiOC_6$), a dye that is taken up into the organelle in a mitochondrial membrane potential (Δψ)–dependent manner (Pringle *et al.*, 1989). To quantify Δψ as a function of mitochondrial mass, we measured the ratio of $DiOC_6$ fluorescence to that of Tom70p-mCherry, a mitochondrial outer membrane protein that is imported into the organelle in a Δψ-independent manner (Pringle *et al.*, 1989; Hughes and Gottschling, 2012).

Initial studies focused on the fitness of all mitochondria within yeast cells. Control studies confirmed that mitochondria are labeled by $DiOC_6$ and that collapse of the Δψ by treatment with the proton ionophore carbonylcyanide *p*-trifluoromethoxyphenylhydrazone (FCCP) results in loss of $DiOC_6$ labeling (Figure 4, A and B). We also find that deletion of *DNM1* results in a significant increase in Δψ (Supplemental Figure S6, A and B). In contrast, mitochondria in *fzo1*Δ (Figure 4, A and B), *mgm1*Δ (Supplemental Figure S4, D and E), and *dnm1*Δ *fzo1*Δ cells (Supplemental Figure S6, A and B), which have no mtDNA, have lower Δψ than mitochondria in wild-type cells. This loss of Δψ is expected because mtDNA encodes respiratory chain components that generate Δψ. Surprisingly, although *fzo1*Δ and *mgm1*Δ cells are *rho*^{0} and do not have mtDNA, the Δψ of mitochondria in *fzo1*Δ or *mgm1*Δ cells is significantly higher than that of mitochondria in *rho*^{0} (*mgm101*Δ) cells bearing wild-type *FZO1* and *MGM1* (Figure 4B). Thus we find that loss of mitochondrial fusion promotes mitochondrial function, as assessed by Δψ, in cells that lack mtDNA.

Loss of mitochondrial fusion promotes inheritance of higher-functioning mitochondria by yeast daughter cells

Because mitochondria are asymmetrically inherited in yeast, and inheritance of fitter mitochondria by yeast daughter cells promotes their lifespan and healthspan (McFaline-Figueroa *et al.*, 2011; Higuchi *et al.*, 2013), we studied the effect of loss of mitochondrial fusion on segregation of fit from less-fit mitochondria during yeast cell division. $DiOC_6$:Tom70p-mCherry ratio imaging revealed that the Δψ of mitochondria in the bud of wild-type cells is 32–56% higher than that of mitochondria in mother cells (Figure 4, C and D, and Supplemental Tables S1–S4). Thus we obtained additional evidence that fitter mitochondria are preferentially inherited by buds. Deletion of *DNM1* and the associated production of a single continuous reticulum of mitochondria mother and daughter cells result in loss of the asymmetry in mitochondrial Δψ between mother cells and buds (Supplemental Figure S6).

Surprisingly, we find that deletion of *FZO1* or *MGM1* promotes inheritance of higher-functioning mitochondria by yeast daughter cells (Figure 4, C and D, and Supplemental Figure S4, F and G). Here too we used *mgm101*Δ *rho*^{0} cells as a control for loss of mtDNA. In *mgm101*Δ cells, there is no obvious difference in the Δψ of mitochondria in mother cells and buds. Thus loss of mtDNA results in loss of the asymmetric inheritance of mitochondria. On the other hand, mitochondria are asymmetrically inherited in *fzo1*Δ or *mgm1*Δ *rho*^{0} cells: Δψ of mitochondria in large buds of *fzo1*Δ or *mgm1*Δ *rho*^{0} cells is 60–92% and 87–144% higher than with mitochondria in mother cells, respectively (Figure 4D, Supplemental Figure S4G, and Supplemental Tables S1 and S3). Indeed, although mitochondria in wild-type cells contain mtDNA and have higher Δψ than mitochondria in *fzo1*Δ and *mgm1*Δ cells, the functional segregation of mitochondria in *fzo1*Δ and *mgm1*Δ *rho*^{0} cells is twofold to threefold greater than that observed in wild-type cells: Δψ of mitochondria in the bud of wild-type cells is only 32–56% higher than that of mitochondria in mother cells. Thus our findings indicate that loss of mitochondrial fusion can promote segregation of fit from less-fit mitochondria.

Increasing mitochondrial anchorage by overexpression of *MMR1* results in inheritance of lower-functioning mitochondria by buds and decreased replicative lifespan

Because Fzo1p and Mgm1p contribute to accumulation of mitochondria in the bud tip and deletion of *FZO1* or *MGM1* results in enhanced recruitment of higher-functioning mitochondria in the bud, it is possible that mitochondrial anchorage has a direct consequence for quality control of the organelle. To test this hypothesis, we studied the effect of increasing mitochondrial anchorage at the bud tip on mitochondrial quality control, using overexpression of *MMR1*. Mmr1p has been shown independently to mediate mitochondrial inheritance in two pathways: first, as an anchor for mitochondria at the bud tip during yeast cell division (Swayne *et al.*, 2011), and second, as an adaptor for Myo2p on mitochondria to promote anterograde transport of the organelle (Eves *et al.*, 2012; Chernyakov *et al.*, 2013).

Initial studies focused on further characterization of Mmr1p and Myo2p function in transport and bud-tip anchorage of mitochondria using the previously characterized *myo2-14* and *mmr1-5* temperature-sensitive mutants (Chernyakov *et al.*, 2013). Consistent with previous reports of Myo2p function in mitochondrial inheritance into the

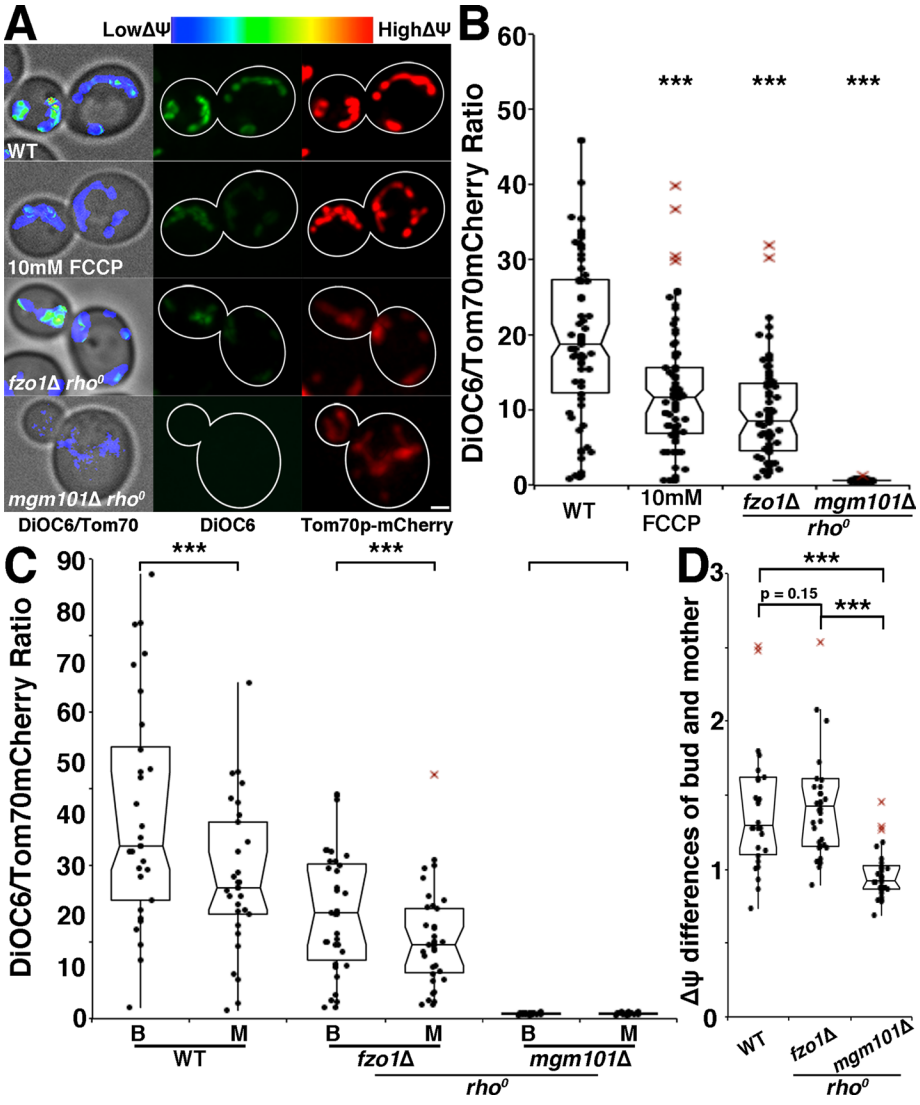

FIGURE 4: Loss of mitochondrial fusion results in decreased overall mitochondrial quality but enhanced segregation of fit from less-fit mitochondria. (A) $DiOC_6$ was used to visualize membrane potential of mitochondria in wild-type, *fzo1Δ rho⁰*, and *mgm101Δ rho⁰* cells. Wild-type cells were treated with 10 mM FCCP for 10 min before $DiOC_6$ staining as a control for loss of membrane potential. $DiOC_6$ intensities were normalized for mitochondrial mass using Tom70-mCherry. Projections of deconvolved wide-field *z*-series. Left, $DiOC_6$:Tom70-mCherry ratio images superimposed on bright-field images. Color scale indicates ratio values; higher numbers and warmer colors indicate higher membrane potential. Middle, $DiOC_6$. Right, Tom70-mCherry. Cell outlines were drawn from bright-field images. Scale bar, 1 μm. (B) Notched dot-box plot of the average $DiOC_6$:Tom70-mCherry ratio in wild-type, FCCP-treated, *fzo1Δ rho⁰*, and *mgm101Δ rho⁰* cells in glucose-based medium. $n = 58–83$ cells for each strain. Data are representative of three experiments. ***$p < 0.001$ vs. wild type using nonparametric Kruskal–Wallis testing with pairwise Bonferroni correction. (C) Notched dot-box plot of the average $DiOC_6$:Tom70-mCherry ratio in bud and mother cells in wild-type, *fzo1Δ rho⁰*, and *mgm101Δ rho⁰* cells in glucose-based medium. Because mother–bud differences are largest late in the cell cycle, measurements for mother–bud differences were performed in yeast cells bearing large buds (0.60–0.80 ratio of bud to mother diameter). ***$p < 0.001$ compared with wild-type using nonparametric Wilcoxon signed-rank testing. (D) Notched dot box plot of ratio of bud:mother DiOC6/Tom70p-mCherry measurements of *fzo1Δ rho⁰* and *mgm101Δ rho⁰* cells. ***$p < 0.001$ using Kruskal–Wallis testing; 29–30 cells/strain. Outliers greater than three times the interquartile range were removed for readability. Two outliers were removed from *fzo1Δ*.

bud, we find that mitochondria in *myo2-14* mutants grown at restrictive temperatures (34°C) undergo linear movements in mother cells but fail to enter the bud (Supplemental Figure S7A; Chernyakov *et al.*, 2013). To further test the roles of Myo2p and Mmr1p in accumulation and maintenance of mitochondria at the bud tip, we grew wild-type, *myo2-14*, and *mmr1-5* cells to mid log phase at permissive temperature (25°C) and then shifted cells to restrictive temperature (34°C). We then assessed whether mitochondria were released from the bud tip in cells that exhibited clear accumulation of mitochondria in the bud tip before the shift from 25 to 34°C. We found that *myo2-14*–mutant cells lose bud-tip anchorage of mitochondria almost immediately after shift to restrictive temperatures (Supplemental Figure S7B). Shift of the *mmr1-5* mutant cells to 34°C also results in release of mitochondria from the bud tip, although the amount of release in *mmr1-5* cells is less than that observed in *myo2-14* mutants (Supplemental Table S5). These data suggest that Myo2p is essential not only for mitochondrial inheritance but also for anchorage of mitochondria at the bud tip and provide additional evidence for a role for Mmr1p in bud-tip anchorage of the organelle.

Consistent with this, we find that a fivefold overexpression of *MMR1* (Supplemental Figure S8A) results in a significant increase in bud-tip accumulation of mitochondria in wild-type cells and rescues the defect in bud-tip mitochondrial accumulation observed in in *fzo1Δ* cells (Figure 5, A and B). Overexpression of *MMR1* in wild-type or *fzo1Δ* cells also results in a decrease in total cellular mitochondrial Δψ. Indeed, the Δψ of mitochondria in *fzo1Δ rho⁰* cells that overexpress *MMR1* is reduced to that of mitochondria in *mgm101Δ rho⁰* cells (Figures 4, A and B, and 5, C and D). Finally, we find that overexpression of *MMR1* abolishes the asymmetric inheritance of mitochondria: the Δψ of mitochondria in mother cells and buds in yeast that overexpress *MMR1* are indistinguishable (Figure 5E). This defect in segregation of mitochondria by fitness during yeast cell division is not due to defects in mitochondrial motility or cytoskeleton-dependent mitochondrial quality control: overexpression of *MMR1* has no effect on mitochondrial motility, actin organization, or RACF (Supplemental Figure S8, B–E). Instead, our findings indicate that increasing accumulation of mitochondria in the bud tip has a negative effect on mitochondrial function and mitochondrial quality control during inheritance.

Because promoting anchorage of mitochondria in the bud results in a decrease in total cellular mitochondrial function, as assessed by Δψ, we tested the effect of *MMR1* overexpression on cellular lifespan and health. Aging studies in yeast can model two distinct forms of cellular aging (Polymenis and Kennedy, 2012). Chronological lifespan, the survival time of stationary-phase,

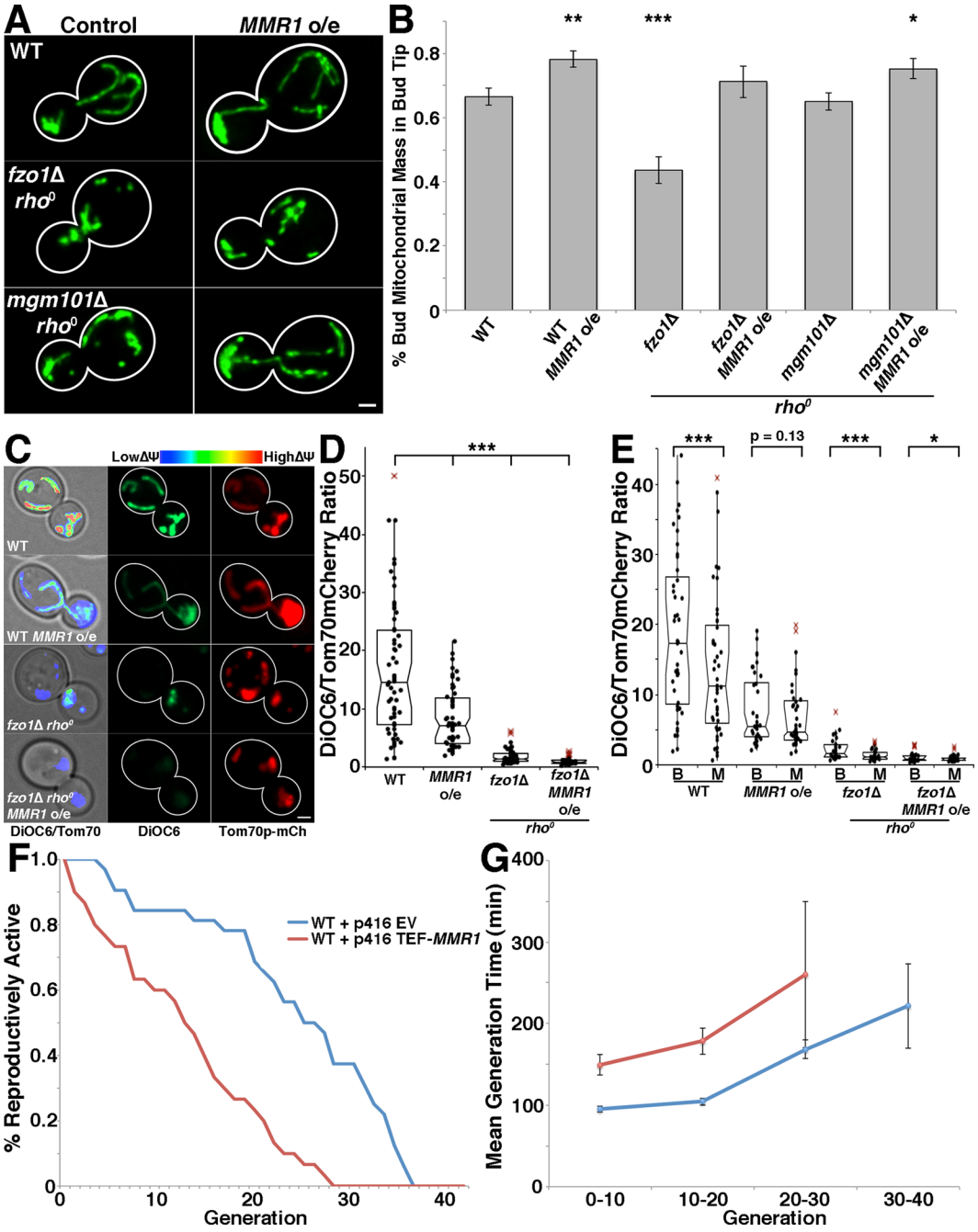

FIGURE 5: Overexpression of *MMR1* increases mitochondrial accumulation at the bud tip, abolishes asymmetrical inheritance of mitochondria, and decreases daughter cell lifespan and healthspan. (A, B) Mitochondrial content in the bud tip was assessed as per Figure 3 for wild-type, *fzo1Δ rho*^{0}, and *mgm101Δ rho*^{0} cells with and without *MMR1* overexpression. Cells were grown in glucose-based medium. *$p < 0.05$, **$p < 0.01$, and ***$p < 0.001$ compared with wild type using Student's *t* test. Data are representative of three experiments; 48–60 cells for each strain. Scale bar, 1 μm. (C) $DiOC_6$ was used to visualize membrane potential of mitochondria as for Figure 4 in wild-type and *fzo1Δ rho*^{0} cells with or without *MMR1* overexpression. Left, $DiOC_6$:Tom70-mCherry ratios superimposed on bright-field images. Color scale indicates ratio values; higher numbers and warmer colors indicate higher membrane potential. Middle, $DiOC_6$. Right,Tom70-mCherry; cell outlines were drawn from bright-field images. Scale bar, 1 μm. (D) Notched dot-box plot of the average $DiOC_6$:Tom70-mCherry ratio in wild-type and *fzo1Δ rho*^{0} cells with or without *MMR1* overexpression. Data are representative of three experiments; 42–65 cells/strain. **$p < 0.001$ using nonparametric Kruskal–Wallis testing with pairwise Bonferroni correction. (E) Notched dot-box plot of the average $DiOC_6$:Tom70-mCherry ratio in bud and mother cells in wild-type and *fzo1Δ rho*^{0} cells with or without *MMR1* overexpression. Data are representative of three experiments. ***$p < 0.001$ and *$p < 0.05$ using nonparametric Wilcoxon signed-rank testing. (F) Replicative lifespan of wild-type cells with either empty vector (EV) or *MMR1* overexpression vector was determined as described in *Materials and Methods*. *p* for average lifespan < 0.001 (Student's t test). (G) Mean generation time was determined during the replicative lifespan assay by recording the time between emergences of consecutive buds from the same mother. Error bars represent SEM. For F and G, 30–32 cells/strain. Data shown are representative of three trials.

nondividing yeast cells, is a model for stress resistance in postmitotic cells. Replicative lifespan (RLS), the number of times that a cell can divide before senescence, is a model for aging of division-competent cells. We find that overexpression of *MMR1* results in a significant decrease in RLS (Figure 5F).

The healthspan of an organism is the period during which it is generally healthy and free of disease or age-related symptoms. Mean generation time, which increases as yeast age, is an indicator of healthspan (Mortimer and Johnston, 1959; McFaline-Figueroa *et al.*, 2011). We find that overexpression of *MMR1* also results in a significant increase in mean generation time (Figure 5G). Thus promoting anchorage of mitochondria in the bud tip by overexpression of *MMR1* results in inheritance of lower-functioning mitochondria, a decrease in mitochondrial function, and decreased lifespan and healthspan.

DISCUSSION

Previous studies indicated that mitochondrial fusion is required for normal mitochondrial morphology, maintenance of mtDNA, and mitochondrial respiratory activity in budding yeast (Hermann *et al.*, 1998; Rapaport *et al.*, 1998). Here we report a novel role for mitochondrial fusion in quantity and quality control of mitochondria at the bud tip.

Role for mitochondrial fusion in mitochondrial quantity control during inheritance through effects on anchorage of the organelle in the bud tip

Our FLIP studies provide direct evidence that mitochondria that move from mother cells to buds can fuse with mitochondria that are anchored in the yeast bud tip. In light of this, we assessed the role of mitochondrial fusion in anchorage of mitochondria in the yeast bud tip. We find that loss of mitochondrial fusion, by deletion of *FZO1*, results in a decrease in the volume of mitochondria that accumulate in the yeast bud tip, a defect in anchorage of mitochondria at that site, and increased retrograde movement of mitochondria away from the bud tip. We also find similar defects in bud-tip accumulation of mitochondria in cells carrying a deletion in the inner membrane fusion mediator, *MGM1*, providing further evidence that the effects we see are due to mitochondrial fusion and not other potential fusion-independent functions of Fzo1p. Overall our data support the model in which mitochondria entering the bud tip fuse with mitochondria that are anchored at that site, generating a continuous reticulum of mitochondria that remain anchored in the bud tip.

Effects of mitochondrial fusion and bud tip anchorage on inheritance of fitter mitochondria by yeast daughter cells

Previous studies revealed that mitochondria that are anchored in the bud tip are higher functioning, that is, are more reducing and have less ROS, compared with mitochondria in mother cells. We obtained additional evidence for this finding: mitochondria in the bud tip also have higher $\Delta\psi$ than mitochondria in mother cells. Our studies also indicate that this segregation of fitter from less-fit mitochondria is not due to preferential binding of higher-functioning mitochondria by the anchorage machinery in the bud tip: anchorage of mitochondria in the bud tip occurs even in *rho*^{0} cells, which have no mtDNA and severely compromised mitochondrial respiratory and protein import activities and $\Delta\psi$.

Consistent with this, we find that promoting anchorage of mitochondria in the bud tip results in increased anchorage of lower-functioning mitochondria at that site and that inhibition of anchorage has the opposite effect. The $\Delta\psi$ of *fzo1*Δ or *mgm1*Δ *rho*^{0} cells are lower than that observed in wild-type cells, which contain mtDNA, as expected because loss of mtDNA result in severe defects in $\Delta\psi$. Surprisingly, we found that mitochondria in *fzo1*Δ *rho*^{0} cells or *mgm1*Δ *rho*^{0} cells are significantly higher functioning overall, as assessed by $\Delta\psi$, than mitochondria in *mgm101*Δ *rho*^{0} cells with normal fusion machinery (i.e., expressing wild-type *FZO1* and *MGM1*). Moreover, in contrast to *rho*^{0} cells, in which there is no detectable asymmetric inheritance of mitochondria, mitochondria in the buds of *fzo1*Δ *rho*^{0} cells or *mgm1*Δ *rho*^{0} cells are fitter than mitochondria in mother cells. Indeed, segregation of fitter from less-fit mitochondria in *fzo1*Δ *rho*^{0} cells or *mgm1*Δ *rho*^{0} cells is twofold to threefold greater than that observed in yeast with wild-type mtDNA (*rho*$^+$ cells). Thus deletion of mitochondrial fusion proteins results in an increase in inheritance of higher-functioning mitochondria by yeast daughter cells and an overall increase in mitochondrial function.

To determine whether the enhanced asymmetric inheritance of mitochondria in the fusion mutants is due to effects on bud tip anchorage, we tested whether promoting bud anchorage of mitochondria by overexpression of Mmr1p compromises asymmetric inheritance of the organelle. Using temperature-sensitive *MMR1* and *MYO2* mutants, we obtained additional evidence for a role for Mmr1p in bud-tip anchorage and for Myo2p in localization of mitochondria to buds. We also obtained evidence for a role of Myo2p in anchorage of mitochondria in the bud tip. Because Myo2p is required for localization of Mmr1p and many other factors to the bud tip, it is possible that it contributes to bud-tip anchorage through its function as a cargo transporter. Equally important, we confirmed that overexpression of *MMR1* increases bud-tip anchorage of mitochondria but has no effect on the frequency or velocity of mitochondrial movement in mother cells. Moreover, we find that promoting anchorage of mitochondria in the bud tip by Mmr1p overexpression abolishes asymmetric inheritance of mitochondria and results in an overall decrease in mitochondrial function, as assessed by $\Delta\psi$, and decreased replicative lifespan and healthspan.

Overall our findings support a novel role for mitochondrial fusion in anchoring mitochondria in the yeast bud tip by mediating fusion of newly inherited mitochondria to mitochondria that are anchored to the bud tip. We also find that mitochondria in the bud are physically distinct from mitochondria in mother cells at late stages in the cell division cycle, which allows mitochondria in buds to be functionally distinct from mitochondria in mother cells and is critical for inheritance of fitter mitochondria by yeast daughter cells after cytokinesis. Finally, we find that fusion-mediated anchorage of mitochondria at the bud tip can counteract mitochondrial quality control during yeast cell division.

Yet to be identified is the mechanism by which *MMR1* overexpression results in decreased mitochondrial quality in the daughter cell. It is possible that promoting inheritance via increased anchorage of mitochondria at the bud tip perturbs quality control mechanisms, such as RACF-mediated removal of damaged mitochondrial from the bud. On the other hand, *MMR1* overexpression may affect other cellular quality control mechanisms, which may have detrimental effects on mitochondrial quality. Indeed, previous reports implicated Myo2p in anterograde transport of both mitochondria and vacuoles and that overexpression of Mmr1p decreases vacuolar volume in the daughter cell (Eves *et al.*, 2012). Because vacuolar maintenance is essential for maintenance of mitochondrial quality (Hughes and Gottschling, 2012; Henderson *et al.*, 2014), it is possible that overexpression of *MMR1* may result in decreased mitochondrial quality in the bud due to vacuolar dysfunction.

The observation that normal inheritance machinery can be detrimental to the organism can be considered counterintuitive. However, this can be reconciled if we consider mitochondrial

quantity and quality control pathways as distinct and complementary processes. The known mitochondrial *quality* control pathways ensure that higher-functioning mitochondria are preferentially transferred from mother to daughter cells or that lower-functioning mitochondria in buds are preferentially repaired or removed. However, they do not monitor the quantity of mitochondria that are inherited by daughter cells. Conversely, the machinery for bud-tip anchorage affects the *quantity* of mitochondria that are anchored in buds and later inherited by daughter cells but does not exercise quality control. Overall it is the balance between quantity and quality control of mitochondrial inheritance that ultimately leads to inheritance of a critical mass of mitochondria that are not necessarily the fittest but are fit enough to ensure that daughter cells are fitter than mother cells, which in turn contributes to mother–daughter age asymmetry. This model is supported by the observations that 1) the quantity of mitochondria in the bud is constant throughout the life cycle, even as the relative mitochondrial content of the other cell decreases (Rafelski *et al.*, 2012), and 2) inhibition of either quantity or quality control pathways leads to shortened lifespan and healthspan (McFaline-Figueroa *et al.*, 2011; Higuchi *et al.*, 2013).

MATERIALS AND METHODS

Yeast growth conditions

S. cerevisiae strains are derivatives of the wild-type BY4741 strains (*MAT***a** *his3Δ1 leu2Δ0 met15Δ0 ura3Δ0*) from Open Biosystems (Huntsville, AL). All imaging experiments were carried out with cultures grown at 30°C with shaking to mid log phase (OD_{600} = 0.1–0.3) in synthetic complete (SC) medium or appropriate dropout or drug-containing medium for selection. For the *dnm1Δ fzo1Δ* strain, cells were grown in glycerol-based medium (SGly-EtOH; 5% glycerol, 3% EtOH) or yeast extract/peptone/glycerol (YPG) to maintain mitochondrial DNA. For all imaging experiments on *dnm1Δ fzo1Δ* cells maintaining mitochondrial DNA, cells were grown in glycerol-based medium and switched to SC, glucose-based medium for 3–4 h before imaging.

Yeast strain construction

In *dnm1Δ*, *fzo1Δ*, and *mgm101Δ* strains, the *DNM1*, *FZO1*, and *MGM101* genes, respectively, were replaced with *LEU2* using primers listed in Supplemental Table S6. A PCR fragment containing regions homologous to sequences directly upstream of the start codon and directly downstream of the stop codon and coding regions for *LEU2* was amplified from plasmid POM13 (Addgene, Cambridge, MA). BY4741 cells were transformed with the PCR product using the lithium acetate method, and transformants were selected on SC-Leu. PCR using specific primers (Supplemental Table S6) was used to confirm deletion of the gene. To produce the *dnm1Δ fzo1Δ rho*$^+$ strain, *FZO1* was replaced with *KanMX-6* amplified by PCR using forward primer 5′-GATATCACGGATAGAGGCAAAACGGTAGGCTCATTTAACGCGGATCCCCGGGTTAATTAA-3′ and reverse primer 5′-TATATTGATTTGAAAAGACCTCATATATTTACAAGAATATGAATTCGAGCTCGTTTAAAC-3′ from plasmid pfa6-KanMX6 (Addgene) in *dnm1Δ* cells and propagated in glycerol-based medium. Transformants were screened by PCR using *fzo1Δ* screening primers (Supplemental Table S6). *dnm1Δ fzo1Δ rho*$^+$ cells were grown in glucose-based medium for >24 h to lose mtDNA. Loss of mtDNA was tested by growth on non–glucose-based medium and 4′,6-diamidino-2-phenylindole (DAPI) staining as described later. All strains used in this study are listed in Supplemental Table S7.

The C-terminus of Cit1p was tagged with GFP(S65T) using PCR-based insertion into the chromosomal copy of *CIT1*. A PCR fragment containing regions homologous to the 3′ end of *CIT1* directly upstream and downstream of the stop codon and coding regions for GFP and the kanamycin resistance marker *kanMX6* was amplified from pFA6a-GFP(S65T) (Addgene,) with forward primer 5′-AAAATACAAGGAGTTGGTAAAGAAAATCGAAAGTAAGAACCGGATCCCCGGGTTAATTAA-3′ and reverse primer 5′-AATAGTCGCATACCCTGAATCAAAAATCAAATTTTCCTTAGAATTCGAGCTCGTTTAAAC-3′. BY4741 cells were transformed with the PCR product using the lithium acetate method, and transformants were selected on yeast extract/peptone/dextrose (YPD) containing 200 µg/ml Geneticin. Cells positive for GFP-tagged Cit1p were screened by fluorescence microscopy.

The C-terminus of Tom70p was tagged with yEpolylinker-mCherry as described. A PCR fragment containing regions homologous to the 3′ end of *TOM70* directly upstream and downstream of the stop codon and coding for yEpolylinker-mCherry and the hygromycin B resistance marker *hphMX4* was amplified from PCY3090-02 (Addgene) using forward primer 5′-TCAAGAAACTTTAGCTAAATTACGCGAACAGGGTTTAATGGGTGACGGTGCTGGTTTA-3′ and reverse primer 5′-TTGTCTTCTCCTAAAAGTTTTTAAGTTTATGTTTACTGTATCGATGAATTCGAGCTCG-3′. Cells positive for yEpolylinker-mCherry-tagged Tom70p were screened by fluorescence microscopy.

MMR1-overexpressing yeast cells were synthesized by expressing p416-TEF-13MYC-*MMR1* as described later. Overexpression was confirmed through Western blot analysis. Whole-cell yeast extracts were prepared by vortexing mid log–phase yeast cells with 0.5-mm glass beads in solution consisting of 10% glycerol, 10 mM ethylene glycol tetraacetic acid, 1% Triton X-100, 50 mM Tris-HCl, pH 7.5, 150 mM NaCl, 2 mM phenylmethonylsulfonylfluoride (PMSF), and protease inhibitor cocktail (Lazzarino *et al.*, 1994). Protein concentration in lysate was determined using the bicinchoninic acid assay following the vendor's protocol (Pierce Chemical, Rockford, IL). 13MYC-tagged Mmr1p levels were analyzed using monoclonal antibody raised against the MYC epitope and in-gel trichloroethanol staining as a loading control (Ladner *et al.*, 2004). Labeled proteins were visualized using Luminata Forte Western HRP Substrate (Millipore, Billerica, MA) on a ChemiDoc imager (Bio-Rad, Hercules, CA).

Plasmid construction

In wild-type yeast cells, the chromosomal locus of *MMR1* was tagged using PCR-based insertion as described. A PCR fragment containing regions homologous to the 5′ end of *MMR1* directly upstream and downstream of the start codon and coding regions for *13MYC* and the auxotrophic marker *LEU2* was amplified from POM43 (Addgene) using forward primer 5′-AAAAAAAAAAACACAACTAATAAACTAAACAACTAAAAAAATGTGCAGGTCGACAACCCTTAAT-3′ and reverse primer 5′-GTTTTGGAGTAAGTTGTTCCGATTTCATTGTTGGAGAATTGCGGCCGCATAGGCCACT-3′. Cells positive for *13MYC*-tagged *MMR1* were screened via PCR using forward primer 5′-GGCACATCTTCCTAAATAGCAGTAAGG-3′ and reverse primer 5′-GCCAGTGTCTAATTTTAGCTTCGTAGG-3′. *13MYC-MMR1* was then PCR amplified from genomic DNA using forward primer 5′-CGCGAAGCTTCCAGTACTCATTGCAAAATCA-3′ and reverse primer 5′-CGCGATCGATTAGCCTACAATACAAAGCGCC-3′. The PCR product and the vector p416-TEF were digested sequentially with *Hin*dIII and *Cla*I and ligated to produce the p416-TEF-*13MYC-MMR1* plasmid.

Microscopy

All wide-field imaging was performed as described previously (Garcia-Rodriguez *et al.*, 2009) on one of the following microscope

systems: an Axiovert 200M microscope with 100×/1.4 Plan-Apochromat objective (Zeiss, Thornwood, NY) and Orca ER cooled charge-coupled device (CCD) camera (Hamamatsu, Bridgewater, NJ); an Axioskop 2 microscope with 100×/1.4 Plan-Apochromat objective (Zeiss, Thornwood, NY) and an Orca 1 cooled CCD camera (Hamamatsu) or an Axiocam CCD camera (Zeiss); or an inverted AxioObserver.Z1 microscope with a 100×/1.3 oil EC Plan-Neofluar objective (Zeiss) and Orca ER cooled CCD camera (Hamamatsu). For visualization of GFP and mCherry, fluorophores were excited by a mercury or metal halide lamp and imaged through standard fluorescein isothiocyanate and rhodamine filter sets. Hardware was controlled by Openlab (PerkinElmer-Cetus, Waltham, MA), Volocity (PerkinElmer-Cetus), Axiovision (Zeiss), or ZEN (Zeiss) software.

Analysis of mitochondrial quality using $DiOC_6$

For determination of mitochondrial membrane potential, yeast cells were stained with $DiOC_6$ as previously described (Hughes and Gottschling, 2012), with some modifications. Cells containing mCherry-tagged Tom70p were grown to mid log phase in SC at 30°C, washed, and resuspended in staining buffer (10 mM 4-(2-hydroxyethyl)-1-piperazineethanesulfonic acid, 5% glucose). A $DiOC_6$ stock solution of 17.5 mM in 100% ethanol was added to a suspension of cells in staining buffer to a final concentration of 17.5 nM. Cells were incubated 15 min with shaking at room temperature, washed three times with staining buffer, concentrated, and mounted on slides and imaged for no more than 2 min. Cells were imaged using a 100×/1.3 EC Plan-Neofluar objective. $DiOC_6$ was excited with a 470-nm LED at 100% power, and emission was imaged using a standard GFP filter (Zeiss filter set 46 HE; dichroic FT 515, emission 535/30). Tom70-mCherry was excited with a metal-halide lamp, and emission was imaged using a standard rhodamine filter (Zeiss filter set 43 HE; excitation 550/25, dichroic FT 570, emission 605/70). *Z*-series were collected through the entire cell at 0.5-µm intervals using 1 × 1 binning. Exposure times were 50 ms for $DiOC_6$ and 200 ms for Tom70-mCherry, with gain at 216. Images were deconvolved using a constrained iterative restoration algorithm with the following parameters: 507-nm emission wavelength, 30 iterations, and 100% confidence limit for $DiOC_6$ and 610-nm emission wavelength, 30 iterations, and 100% confidence limit for Tom70-mCherry. $DiOC_6$-to-Tom70-mCherry ratios were calculated by dividing, pixel by pixel, the intensity of $DiOC_6$ by that of Tom70-mCherry after background selection and thresholding. Zones of mother and bud were identified using corresponding transmitted-light images.

Because $DiOC_6$/Tom70-mCherry data are not normal using the Shapiro–Wilk statistical analysis for normality, notched dot-box plots and nonparametric statistical analysis were used to determine *p* values. The percentage differences in $DiOC_6$/Tom70-mCherry ratios were obtained by taking the average (mean) values of $DiOC_6$/Tom70-mCherry ratios of the bud and mother cell independently and then calculating ratios of those means. Because there is cell-to-cell variability in Tom70-mCherry expression, all data were normalized on an individual cell basis. The calculated ratios of bud to mother $DiOC_6$/Tom70-mCherry values were obtained, and data were represented as $\Delta\psi$ differences between bud and mother. Raw data are given as notched dot-box plots for the most relevant strains in Figure 4D and Supplemental Figure S2G. The averages of these individually calculated ratios for all strains are shown in Supplemental Table S1.

Fluorescence loss in photobleaching

FLIP experiments for Figures 1 and 4 were performed on a Leica TCS MP5 laser scanning confocal microscope (Leica Microsystems US, Buffalo Grove, IL). Wild-type yeast expressing mitochondrial matrix–targeted GFP were concentrated and mounted on slides as described. Bleaching was performed with the 488-nm laser line on a spot within mitochondria in the bud. Imaging was carried out simultaneously with bleaching at 0.47-s intervals for a total of 48 s. Quantification was performed by drawing ROIs around tubular mitochondrial structures or in manually drawn ROIs where specified and calculating integrated pixel intensities. FLIP experiments for Figure 2 were performed on a Nikon A1R-MP laser scanning confocal microscope (Nikon Instruments, Melville, NY). Wild-type yeast expressing mitochondrial matrix–targeted GFP were concentrated and mounted on slides as described. Bleaching was performed with the 488-nm laser line on a circular spot 0.5 µm in diameter within mitochondria at the bud tip. A cycle consisting of 125 ms of photobleaching and 250 ms of imaging was repeated for a total of 12 s. Quantification was performed by drawing ROIs around tubular mitochondrial structures or in manually drawn ROIs where specified and calculating integrated pixel intensities.

Quantitation of the velocity and frequency of mitochondrial movement

Yeast expressing mitochondrial targeted redox-sensitive GFP were visualized using 470-nm LED excitation at 100% power and a standard GFP filter set. Single-plane images (focused at the center of the mother cell) were recorded at 1-s intervals for a total of 30 s using 1 × 1 binning, 75 ms exposure, and gain at 216. The change in position of the tip of each moving or elongating tubular mitochondrion was recorded as a function of time. Mitochondrial movement was scored when a mitochondrion made three or more consecutive movements in the same direction. Image enhancement and analysis were performed using Volocity software.

Measurements of mitochondrial distribution

Mitochondria were visualized in living cells using GFP-tagged Cit1p. Cells were grown to mid log phase in SC and concentrated by centrifugation at 4656 × *g*, and 1.5 µl of cell suspension was applied to a microscope slide and imaged immediately for a maximum of 15 min after slide preparation. Cit1-GFP was excited with a 470-nm LED at 100% power, and emission was imaged using a standard GFP filter. *Z*-series were collected through the entire cell at 0.5-µm intervals using 1 × 1 binning and 150-ms exposure time at 216 gain. Images were deconvolved using a constrained iterative restoration algorithm with the following parameters: 507-nm emission wavelength, 30 iterations, and 100% confidence limit. The bud was divided in half by a plane parallel to the bud site, creating the bud tip (the area from the center of the bud to the bud tip distal to the mother cell) and the bud neck (the area from the center of the bud to the boundary with the mother cell). The mother cell was divided into three parts by dividing its long axis into three equal segments with perpendicular planes, creating the mother neck (the area proximal to the bud–mother boundary), the mother middle (the central zone of the mother), and the mother tip (the area most distal to the bud). The relative mitochondrial mass was determined in each region using Volocity software by measuring integrated intensity of mitochondria and normalizing to the total integrated intensity of the mitochondria within the entire cell.

Visualization of F-actin with rhodamine–phalloidin

Visualization of actin with rhodamine–phalloidin was performed as previously described (Higuchi *et al.*, 2013). Briefly, cells were grown to mid log phase in YPD at 30°C and fixed by adding paraformaldehyde to 3.7% into the growth medium. Cells continued to incubate

at 30°C for 50 min. Fixed cells were washed three times with wash solution (0.025 M KPi, pH 7.5, 0.8 M KCl) followed by one wash with PBT (1× PBS containing 1% [wt/vol] bovine serum albumin, 0.1% [vol/vol] Triton X-100, 0.1% [wt/vol] sodium azide) and stained with 1.65 μM rhodamine–phalloidin (Molecular Probes, Eugene, OR) for 35 min at room temperature in the dark. Cells were washed three times with 1× PBS, resuspended in mounting solution, and stored at −20°C until visualization. Rhodamine–phalloidin was visualized using a 100×/1.3 EC Plan-Neofluar objective using a metal-halide lamp for excitation and a standard rhodamine filter (Zeiss filter set 43 HE; excitation 550/25, dichroic FT 570, emission 605/70). *Z*-series were collected through the entire cell at 0.3-μm intervals using 1 × 1 binning and 150-ms exposure. Images were deconvolved using a constrained iterative restoration algorithm (Volocity) with 620-nm emission wavelength, 60 iterations, and 100% confidence limit.

Measurement of retrograde actin cable flow

Cells were grown to mid log phase in SC medium, and 1.5 μl of concentrated cell suspension was spread over the surface of a glass slide and covered with a coverslip. Slides were imaged within 2 min after slide preparation. Abp140p-GFP was imaged using a Zeiss 100×/1.4 Plan-Apochromat objective lens using a metal-halide lamp and a standard GFP filter (Zeiss filter set 46 HE; dichroic FT 515, emission 535/30). Images were collected at a focal plane of ~0.5 1 μm above the center of the mother cell at 0.524-s intervals for a total of 10 s using 1 × 1 binning, 300 ms exposure, and analogue gain of 216.

The velocity of RACF was determined by measuring the change in position of the tip of a moving or elongating cable or the movement of bright fiduciary marks along actin cables as a function of time as previously described (Yang and Pon, 2002). Image analysis and enhancement were performed using Volocity software.

Assessment of mitochondrial genome maintenance

Aliquots of serial dilutions were spotted on both YPD and YPG plates. Failure to grow on medium containing a nonfermentable carbon source as a sole carbon source (YPG) indicates loss of mitochondrial respiration. Visualization of mtDNA was performed on cells fixed as described and resuspended in mounting solution containing 0.5 μg/ml DAPI. Stained cells mounted on microscope slides were imaged using a 100×/1.3 EC Plan-Neofluar objective (Carl Zeiss), 365 nm LED at 100% power using a standard DAPI filter (Zeiss filter set 49; excitation G365, dichroic FT 395, emission 445/50). *Z*-series were collected through the entire cell at 0.3-μm intervals using 1 × 1 binning and 25-ms exposure time. Images were deconvolved using a constrained iterative restoration algorithm with 460-nm emission wavelength, 30 iterations, and 100% confidence limit.

Spinning-disk confocal imaging

Analysis of mitochondrial retention at the bud tip in *mmr1-5* and *myo2-14* temperature-sensitive mutants was carried out on a CSU-X1 spinning-disk confocal attachment (Yokogawa, Sugar Land, TX) on a Ti Eclipse microscope stand (Nikon Instruments) with a stage-mounted piezo focus drive (Mad City Labs, Madison, WI), using a 100×/1.45 Plan-Apo Lambda objective lens and an Evolve electron-multiplying CCD camera (Photometrics, Tucson, AZ). Temperature was maintained by a stage-top incubator and objective heater (Tokai Hit, Shizuoka-ken, Japan). Cells expressing Cit1-GFP were grown to mid log phase at 25°C, concentrated, mounted on agar pads on glass slides, and imaged at 3-min intervals at 34°C for 90 min. Spinning-disk confocal z-series were collected through the middle 3 μm of the cell at 0.5-μm intervals.

Assessment of replicative lifespan

Replicative lifespan measurements were performed as previously described, without α-factor synchronization. Briefly, frozen yeast strain stocks (stored at −80°C) were grown on SC-URA plates at 30°C. Single colonies of wild-type cells harboring either an empty p416-TEF vector or P416-TEF-*13MYC-MMR1* overexpression vector were individually suspended in liquid SC-URA and grown at 30°C with shaking to mid log phase (OD_{600} = 0.1–0.3). A 2-μl aliquot of cell suspension was applied to a SC-URA plate. Small-budded cells were isolated and arranged in a matrix using a micromanipulator mounted on a SporePlay model 000000123 dissecting microscope (Singer Instruments, Watchet, United Kingdom). When the small buds completed growth, their mother cells were removed and discarded, and the remaining daughter cells were named virgin mother cells. After each subsequence replication, the time and number of daughter cells produced by each virgin mother cell were recorded until all replication ceased.

Statistical methods

All statistical testing, production of box plots, and determination of *p* values were performed using the Analyse-it add-on (Analyse-it Software, Leeds, United Kingdom) for Excel (Microsoft, Redmond, WA). Nonparametric Kruskal–Wallis, Wilcoxon signed-rank, and Mann–Whitney *U* testing, as well as parametric Student's *t* test and chi-square testing, were used to calculate *p* values where appropriate and as detailed in each figure legend. For all notched dot-box plots, the central band in the box represents the median, and boxes indicate the middle quartiles; whiskers extend to the 5th and 95th percentiles, black dots represent all data points, and red crosses indicate outliers (defined as quartile 1 − 1.5× interquartile range and quartile 3 + 1.5× interquartile range)

Analysis of mitochondrial connectivity in mother versus bud

Cells were imaged and mitochondria skeletonized as described in Rafelski *et al*. (2012). The data set represents three separate days of experiments and includes a total of 134 budding cells. Unbudded cells in G1 were ignored for this analysis. Bud size was converted into percentage progression of budding as in Rafelski *et al*. (2012) and Higuchi *et al*. (2013). Cells were then further categorized based on their percentage progression of budding as follows: small buds (0–25%), medium-small buds (25–50%), medium buds (50–75%), and large buds (>75%). The length of the mitochondria in mothers and buds was calculated as the length of the skeleton of the mitochondria in each compartment. The mitochondrial network in a cell can be anything from one single interconnected structure to many small individual tubules. Each interconnected structure is defined as a connected component when considering the mitochondria as a mathematical network. The length of the largest connected component is therefore simply the length of the largest continuous structure. This was calculated for each mother and bud. The number of cells displaying a continuous structure extending from the mother to any part of the bud was also calculated. To calculate the percentage of mitochondria that are interconnected in the mother and the bud, respectively, the length of mitochondria in the largest connected component was divided by the total length of mitochondria in that compartment.

ACKNOWLEDGMENTS

We thank the members of the Pon laboratory for technical assistance and valuable discussion, Julie Canman and Tim Davies (Columbia University, New York, NY) for access to the Therminator (Davies *et al.*, 2014) and assistance with the studies on temperature-sensitive yeast mutants, and Anthony Bretscher (Cornell University, Ithaca, NY) for yeast strains. This work was supported by grants from the National Institutes of Health (GM45735 and GM096445) and the Ellison Medical Foundation (AG-SS-2465-10) to L.P., awards from the National Science Foundation (MCB-1330451) and Ellison Medical Foundation (AG-NS-1023-13) to S.M.R., the National Institutes of Health (5 T32 DK7647) to R.H.S., the National Institutes of Health (5 T32 GM007367) to E.J.G., and the Amgen Foundation to A.K. One of the microscopes used for this study was obtained using a National Institutes of Health Shared Instrumentation Grant (S10RR025686). Two of the microscopes used for these studies are supported in part through National Institutes of Health/National Cancer Institute Grant 5 P30 CA13696.

REFERENCES

Bleazard W, McCaffery JM, King EJ, Bale S, Mozdy A, Tieu Q, Nunnari J, Shaw JM (1999). The dynamin-related GTPase Dnm1 regulates mitochondrial fission in yeast. Nat Cell Biol 1, 298–304.

Chen XJ, Guan MX, Clark-Walker GD (1993). MGM101, a nuclear gene involved in maintenance of the mitochondrial genome in Saccharomyces cerevisiae. Nucleic Acids Res 21, 3473–3477.

Chernyakov I, Santiago-Tirado F, Bretscher A (2013). Active segregation of yeast mitochondria by Myo2 is essential and mediated by Mmr1 and Ypt11. Curr Biol 23, 1818–1824.

Davies T, Jordan SN, Chand V, Sees JA, Laband K, Carvalho AX, Shirasu-Hiza M, Kovar DR, Dumont J, Canman JC (2014). High-resolution temporal analysis reveals a functional timeline for the molecular regulation of cytokinesis. Dev Cell 30, 209–223.

Egilmez NK, Jazwinski SM (1989). Evidence for the involvement of a cytoplasmic factor in the aging of the yeast Saccharomyces cerevisiae. J Bacteriol 171, 37–42.

Eves PT, Jin Y, Brunner M, Weisman LS (2012). Overlap of cargo binding sites on myosin V coordinates the inheritance of diverse cargoes. J Cell Biol 198, 69–85.

Garcia-Rodriguez LJ, Crider DG, Gay AC, Salanueva IJ, Boldogh IR, Pon LA (2009). Mitochondrial inheritance is required for MEN-regulated cytokinesis in budding yeast. Curr Biol 19, 1730–1735.

Guo X, Macleod GT, Wellington A, Hu F, Panchumarthi S, Schoenfield M, Marin L, Charlton MP, Atwood HL, Zinsmaier KE (2005). The GTPase dMiro is required for axonal transport of mitochondria to Drosophila synapses. Neuron 47, 379–393.

Henderson KA, Hughes AL, Gottschling DE (2014). Mother-daughter asymmetry of pH underlies aging and rejuvenation in yeast. Elife 3, e03504.

Hermann GJ, Thatcher JW, Mills JP, Hales KG, Fuller MT, Nunnari J, Shaw JM (1998). Mitochondrial fusion in yeast requires the transmembrane GTPase Fzo1p. J Cell Biol 143, 359–373.

Higuchi R, Vevea JD, Swayne TC, Chojnowski R, Hill V, Boldogh IR, Pon LA (2013). Actin dynamics affect mitochondrial quality control and aging in budding yeast. Curr Biol 23, 2417–2422.

Hughes AL, Gottschling DE (2012). An early age increase in vacuolar pH limits mitochondrial function and lifespan in yeast. Nature 492, 261–265.

Itoh T, Toh EA, Matsui Y (2004). Mmr1p is a mitochondrial factor for Myo2p-dependent inheritance of mitochondria in the budding yeast. EMBO J 23, 2520–2530.

Katajisto P, Dohla J, Chaffer CL, Pentinmikko N, Marjanovic N, Iqbal S, Zoncu R, Chen W, Weinberg RA, Sabatini DM (2015). Stem cells. Asymmetric apportioning of aged mitochondria between daughter cells is required for stemness. Science 348, 340–343.

Kennedy BK, Austriaco NR Jr, Guarente L (1994). Daughter cells of Saccharomyces cerevisiae from old mothers display a reduced life span. J Cell Biol 127, 1985–1993.

Koshiba T, Detmer SA, Kaiser JT, Chen H, McCaffery JM, Chan DC (2004). Structural basis of mitochondrial tethering by mitofusin complexes. Science 305, 858–862.

Ladner CL, Yang J, Turner RJ, Edwards RA (2004). Visible fluorescent detection of proteins in polyacrylamide gels without staining. Anal Biochem 326, 13–20.

Lazzarino DA, Boldogh I, Smith MG, Rosand J, Pon LA (1994). Yeast mitochondria contain ATP-sensitive, reversible actin-binding activity. Mol Biol Cell 5, 807–818.

McFaline-Figueroa JR, Vevea J, Swayne TC, Zhou C, Liu C, Leung G, Boldogh IR, Pon LA (2011). Mitochondrial quality control during inheritance is associated with lifespan and mother-daughter age asymmetry in budding yeast. Aging Cell 10, 885–895.

Meeusen S, DeVay R, Block J, Cassidy-Stone A, Wayson S, McCaffery JM, Nunnari J (2006). Mitochondrial inner-membrane fusion and crista maintenance requires the dynamin-related GTPase Mgm1. Cell 127, 383–395.

Mortimer RK, Johnston JR (1959). Life span of individual yeast cells. Nature 183, 1751–1752.

Palay SL (1956). Synapses in the central nervous system. J Biophys Biochem Cytol 2, 193–202.

Polymenis M, Kennedy BK (2012). Chronological and replicative lifespan in yeast: do they meet in the middle? Cell Cycle 11, 3531–3532.

Pringle JR, Preston RA, Adams AE, Stearns T, Drubin DG, Haarer BK, Jones EW (1989). Fluorescence microscopy methods for yeast. Methods Cell Biol 31, 357–435.

Quintana A, Schwindling C, Wenning AS, Becherer U, Rettig J, Schwarz EC, Hoth M (2007). T cell activation requires mitochondrial translocation to the immunological synapse. Proc Natl Acad Sci USA 104, 14418–14423.

Rafelski SM, Viana MP, Zhang Y, Chan YH, Thorn KS, Yam P, Fung JC, Li H, Costa Lda F, Marshall WF (2012). Mitochondrial network size scaling in budding yeast. Science 338, 822–824.

Rapaport D, Brunner M, Neupert W, Westermann B (1998). Fzo1p is a mitochondrial outer membrane protein essential for the biogenesis of functional mitochondria in Saccharomyces cerevisiae. J Biol Chem 273, 20150–20155.

Shepard KA, Gerber AP, Jambhekar A, Takizawa PA, Brown PO, Herschlag D, DeRisi JL, Vale RD (2003). Widespread cytoplasmic mRNA transport in yeast: identification of 22 bud-localized transcripts using DNA microarray analysis. Proc Natl Acad Sci USA 100, 11429–11434.

Sinclair DA, Guarente L (1997). Extrachromosomal rDNA circles—a cause of aging in yeast. Cell 91, 1033–1042.

Stowers RS, Megeath LJ, Gorska-Andrzejak J, Meinertzhagen IA, Schwarz TL (2002). Axonal transport of mitochondria to synapses depends on milton, a novel Drosophila protein. Neuron 36, 1063–1077.

Swayne TC, Zhou C, Boldogh IR, Charalel JK, McFaline-Figueroa JR, Thoms S, Yang C, Leung G, McInnes J, Erdmann R, Pon LA (2011). Role for cER and Mmr1p in anchorage of mitochondria at sites of polarized surface growth in budding yeast. Curr Biol 21, 1994–1999.

Verstreken P, Ly CV, Venken KJ, Koh TW, Zhou Y, Bellen HJ (2005). Synaptic mitochondria are critical for mobilization of reserve pool vesicles at Drosophila neuromuscular junctions. Neuron 47, 365–378.

Yang HC, Palazzo A, Swayne TC, Pon LA (1999). A retention mechanism for distribution of mitochondria during cell division in budding yeast. Curr Biol 9, 1111–1114.

Yang HC, Pon LA (2002). Actin cable dynamics in budding yeast. Proc Natl Acad Sci USA 99, 751–756.